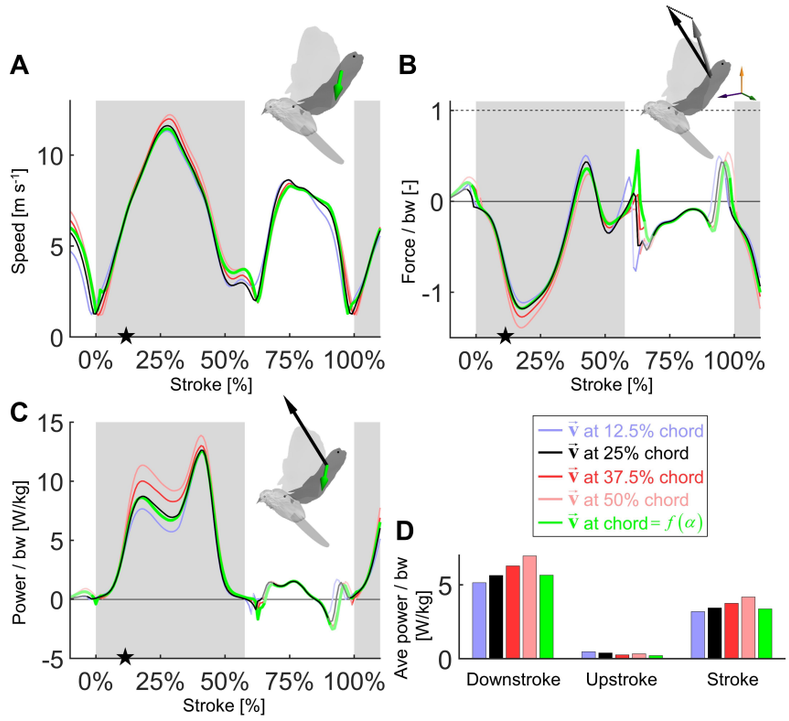

Fig S1. Sensitivity of the time-resolved aerodynamic power to the estimated chord-wise location of the center of pressure. We adopt the same notation for displaying results based on the quarter-chord (25% chord) velocity method (solid line) as in the main text. The most detailed calculation of aerodynamic power (green line) is based on estimating the center of pressure at each chord section based on the measured local angle of attack (α), which allows us to predict the center of pressure according to the quasi-steady model developed for flapping wings; Eq. 20 in (Dickson et al., 2008). We also made power calculations for fixed centers of pressure closer to the leading edge of the wing (12.5% is colored light blue) and closer to the trailing edge of the wing (colored red; 37.5% is red, and 50% is light red) to demonstrate the sensitivity of our calculations. A center of pressure at 12.5% corresponds to an angle of attack of 16 degrees, and 50% corresponds to 99 degrees (Dickson et al., 2008), which are beyond the extremes that we measured in angle of attack (Fig. S3A). (A) The magnitude of the representative wing velocity as a function of stroke phase (plotted as in Fig. 1D). (B) The computed lateral aerodynamic force normalized by bodyweight (plotted as in Fig. 2D). (C) The total aerodynamic power per unit bodyweight (plotted as in Fig. 3B). (D) The average specific aerodynamic power per unit bodyweight plotted as in Fig. 3C. (Gray region, downstroke; force normalized by bodyweight, bw; faded lines correspond to filtered regions with singularity, the red regions in Fig. 2C)

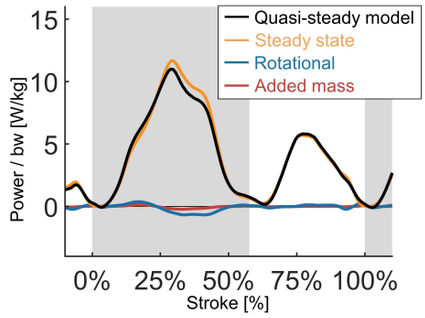

Fig S2. Breakdown of quasi-steady model contributions to aerodynamic power. The power calculation based on *in vivo* aerodynamic force and kinematics measurements can be approximated using the quasi-steady model (Dickson et al., 2008), which gives a stroke-resolved power prediction as well as a stroke-averaged value. The quasi-steady prediction (Dickson et al., 2008) is based on the 3D surface measurement of the dove's wing; the time- and spanwise-resolved wing chord, angles of attack, and velocity vectors. To estimate the spanwise resolved steady state lift and drag coefficients, we combine the spanwise angle of attack and lift-drag polars (both the positive and negative polar) for a hummingbird (*Calypte anna*) wing (Kruyt et al., 2014) as an approximation. (Gray region, downstroke; power normalized by bodyweight, bw)

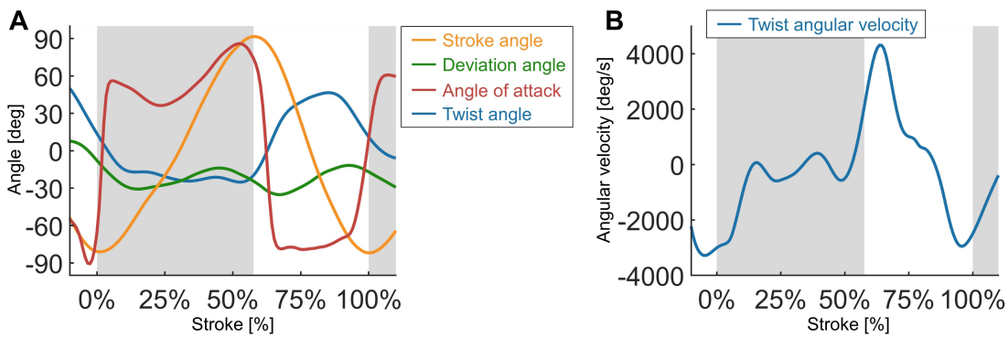

Fig S3. Stroke-resolved wing stroke, deviation, angle of attack and twist kinematics. (A) The wing stroke angle (orange), deviation angle (green), angle of attack (red) and twist angle (blue) are plotted versus stroke phase during the 2nd wingbeat. The corresponding stroke plane is pitched down over 25 degrees with respect to the horizontal (about the y axis; Fig 1B), which we determined based on a linear fit of the tip of the 9th primary feather throughout the full wingbeat. See Fig. 6 in Ingersoll and Lentink 2018 (Ingersoll and Lentink, 2018) for a standard diagram showing the angle definitions that we adopt here with respect to the stroke plane. (B) The angular velocity of wing twist peaks near the downstroke-upstroke transition. (Gray region, downstroke)

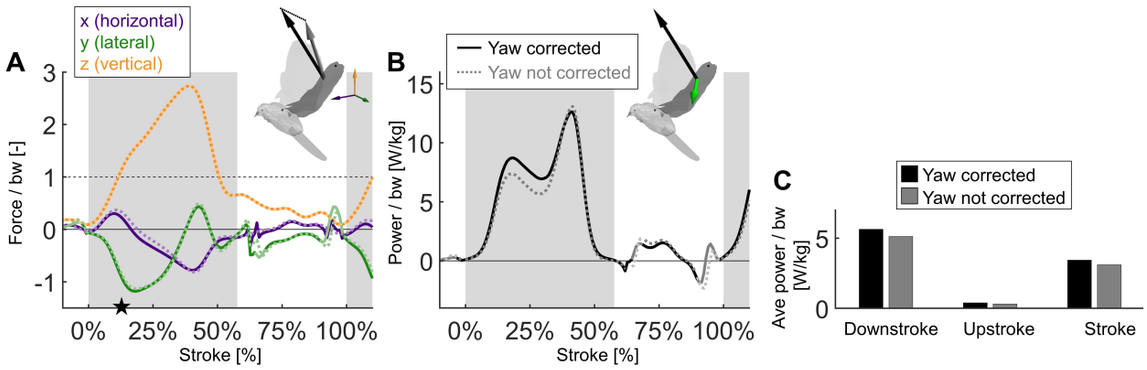

Fig S4. Including body yaw angle improves the accuracy of aerodynamic power calculation. The aerodynamic force and power are plotted for two cases: The dotted lines are computed assuming that the bird had zero body yaw relative to the world reference frame $\theta = 0°$ (Eqns 12-13). The solid lines are computed using the measured body yaw angle (Eqns 14-15; Appendix A3) of $\theta = 6.8°$ based on the dove's tracked kinematics. (A) The x, y, and z components of the aerodynamic force per unit bodyweight vector plotted as in Fig. 2D. (B) The total aerodynamic power per unit bodyweight plotted as in Fig. 3B. (C) The average specific aerodynamic power per unit bodyweight plotted as in Fig. 3C. (Gray region, downstroke; faded lines correspond to filtered regions with singularity, the red regions in Fig. 2C)